Journal of Bio- and Tribo-Corrosion (2025) 11:95
https://doi.org/10.1007/s40735-025-01010-y

Evaluation of Corrosion Resistance of a Sol–Gel Derived Non-stoichiometric Amorphous Aluminum Phosphate Coating in NaCl, and Sulfuric Acid Solutions

Tara Bazdar[1] · Abdoulmajid Eslami[1] · Ahmad Monshi[1] · Fatemeh Sadat Sayyedan[2]

Received: 2 February 2024 / Revised: 27 June 2025 / Accepted: 7 July 2025

Abstract
This study investigates the corrosion resistance of an aluminum phosphate sol–gel derived non-stoichiometric coating in the standard 3.5 wt.% NaCl solution, and also in an industrial 18 wt.% H_2SO_4 solution. Phase analysis of the coating was performed by regular X-ray diffraction (XRD), and grazing incidence X-ray diffraction (GI-XRD) techniques, and also surface observations were performed by scanning electron microscope (SEM). The corrosion resistance of the obtained coating was then investigated using potentiodynamic polarization and electrochemical impedance spectroscopy (EIS) test methods. Results showed by applying the $AlPO_4$ amorphous coating on the AISI 304 stainless steel substrate, corrosion current density (i_{corr}) in the 3.5% NaCl environment decreased significantly from 3.5×10^{-7} to 9.12×10^{-9} A/cm^2, and, mitigated from 1.67×10^{-6} to 1.58×10^{-7} A/cm^2 in the 18 wt.% H_2SO_4 aqueous solution. This was explained by the different corrosion mechanisms in saline and acidic environments, as well as the ceramic nature and lack of grain boundaries due to the amorphous structure of the coating.

Keywords Amorphous coating · Aluminum phosphate · Corrosion resistance · Electrochemical impedance spectroscopy

1 Introduction

Corrosion is the most critical factor in the failure of industrial equipment. Lack of metal surface protection in harsh corrosive environments results in a significant loss in industries [1]. Protection of metals' surface with an effective coating is the most preferred anti-corrosion method due to its reliable and economical aspect [2]. Due to their superior mechanical properties and excellent high temperature and corrosion resistance, advanced ceramics have been investigated in recent decades and are widely used as a coating for protecting base metals in various applications and conditions [3, 4]. As one of the advanced ceramics, chemically bonded phosphate ceramics (CBPCs) show significant efficiency in harsh corrosive environments [5–7]. CBPC materials are manufactured through a reaction between acidic phosphorous and a divalent or trivalent cation and can be synthesized by the sol–gel technique [8–10].

Aluminum phosphates, one of the several types of CBPCs, are well-known as binders and show remarkable performance as inorganic protective coatings after heat treatment at relatively elevated temperatures [11]. Moreover, $AlPO_4$ and other related components have noticeable thermal and chemical stability, good corrosion resistance, and high-temperature oxidation resistance [12]. $AlPO_4$ is commonly amorphous in ambient and low temperatures and can have either crystalline or amorphous structures depending on Al/P molar ratios and heat-treatment temperatures. The crystalline form of $AlPO_4$ has significant iso-structural similarity with the SiO_2 crystalline structure and its polymorphs [13, 14]. Because of stresses caused by polymorphic transformations in the crystalline structure of $AlPO_4$, similar to the changes observed in quartz, the use of non-stoichiometric molar ratios to achieve an amorphous structure is suggested. Amorphous materials also have good corrosion resistance due to the lack of grain boundaries which are active regions for corrosion reactions. Amorphous structures

✉ Abdoulmajid Eslami
m.eslami@cc.iut.ac.ir

[1] Department of Materials Engineering, Isfahan University of Technology, Isfahan 84156-83111, Iran

[2] Department of Materials Science and Engineering, Faculty of Engineering, Ferdowsi University of Mashhad, Mashhad 9177948944, Iran

Published online: 30 July 2025

with high-temperature stability are intelligibly achievable through the sol–gel method by fabricating the precursors with different Al/P molar ratios [15].

There has been some literature investigating amorphous aluminum phosphate properties. In this regard, Maharana et al. [16]. synthesized a nearly amorphous sol–gel derived $Al_{1+x}PO_{4+3x/2}$ matrix using aluminum nitrate and phosphorous pentoxide in ethanolic solution, which preserved its amorphous structures up to 900 °C. Li et al. [17] fabricated amorphous $AlPO_4$ by the polyesterification reaction between P_2O_5 and $Al(NO_3)_3$ ethanolic solution, with its amorphous structure lasting up to 900 °C. Moreover, Sayyedan et al. [12] applied a non-stoichiometric $AlPO_4$ coating on the surface of stainless steel AISA 304, with an Al:P ratio of 1.75:1 using the precursors mentioned before. The high-temperature oxidation resistance of the coating compared to the bare substrate, was reported.

Although $AlPO_4$ coating has shown acceptable corrosion resistance in some environments [18], no research has been conducted on the corrosion resistance of this coating in acidic solutions. Considering that sulfuric acidic solution is used in various industries such as steel and copper industries, the purpose of this research is to investigate the corrosion resistance of non-stoichiometric amorphous $AlPO_4$ coating synthesized by the sol–gel derived method in two different environments, namely the standard 3.5 wt.% NaCl and also an industrial sulfuric acidic solution (18 wt.% H_2SO_4 solutions with some percentage of Cu impurities), as compared to the corrosion resistance of the commonly used AISI 304 Stainless Steel in these environments.

2 Materials and Methods

2.1 Aluminum Phosphate Preparation

First, a sol–gel precursor solution for fabricating amorphous aluminum phosphate was synthesized by dissolving specific amounts of aluminum nitrate nonahydrate ($Al(NO_3)_3{\cdot}9H_2O$, Merck, 98.5% purity) and orthophosphoric acid (H_3PO_4, Merck, 98% purity) separately in ethanol (C_2H_5OH, Merck, 99.8% purity). Then, the phosphorous-based ethanolic solution was added to the aluminum-based ethanolic solution and stirred for 4 h. As the mixing was completed and the solution became clear, it was heated up to 75 °C for 15 min and consequently cooled in the air while stirring. Then, 5 wt.% polyvinylpyrrolidone (PVP, Sigma-Aldrich, molecular weight = 40,000) was added to the solution and stirred until complete dissolution.

2.2 Substrate Preparation and Coating Application

AISI 304 stainless steel substrate was cut into 20 × 20 × 1 mm pieces, then ground gradually using SiC grinding papers up to 2500 grit and polished using fine alumina slurry. Prior to applying the coating, specimens were washed with deionized water and degreased ultrasonically in an acetone bath for 20 min, then rinsed and blow-dried immediately. Aluminum phosphate solution was applied to the substrates by dip coating process with a constant rate of 15 mm min^{-1}. The coated specimens were then dried overnight at 65 °C and then calcined in air at 500 °C for 15 min. The calcination process was employed not only to remove volatile organic components but also to stabilize the amorphous microstructure and enhance corrosion resistance [17]. After heat treatment, the surface of the specimens was smooth and glossy without any inequality. In addition, part of the gel was dried at 60 °C for 24 h and heat-treated at 500 °C for 15 min for further characterizations.

2.3 Coating Characterization

The phase composition of the powder was analyzed using X-ray diffractometry (XRD, PMD Philips X-Pert) with Ni-filtered Cu Ka (Cu Ka = 0.154 nm, radiation at 40 kV and 30 mA) over the 2θ range of 10–90° (time per step: 1.25 s). The grazing incidence XRD (GIXRD) was also performed to determine the phase composition of the heat-treated coatings with an angle of 1° to prevent collecting intense signals of the substrate. The surface morphology of the coating was observed using scanning electron microscopy (SEM, Philips Xl30 equipped with energy dispersive X-ray spectrometer (EDS), EDX Silicon Drift). Cross-sectional SEM imaging was also performed to directly observe the coating structure and confirm its uniformity.

2.4 Electrochemical Analysis

Amorphous aluminum phosphate-coated specimens were electrochemically analyzed to study their corrosion resistance. Electrochemical measurements of the coatings were conducted in the standard 3.5 wt.% NaCl, as well as an industrial sulfuric acid solution (18 wt.% H_2SO_4 aqueous solution with some percentage of cu and Fe impurities[1]). The measurements were carried out using AMETEK PARSTAT 2237 potentiostat/galvanostat system in a standard three-electrode cell apparatus, including a Pt electrode as the counter electrode and a saturated Ag/AgCl as the

[1] The industrial sulfuric acid solution was obtained from a Cu refinery industry with chemical composition of 18 wt.% H_2SO_4, 4.5 wt.% Cu, 2 wt.% Fe.

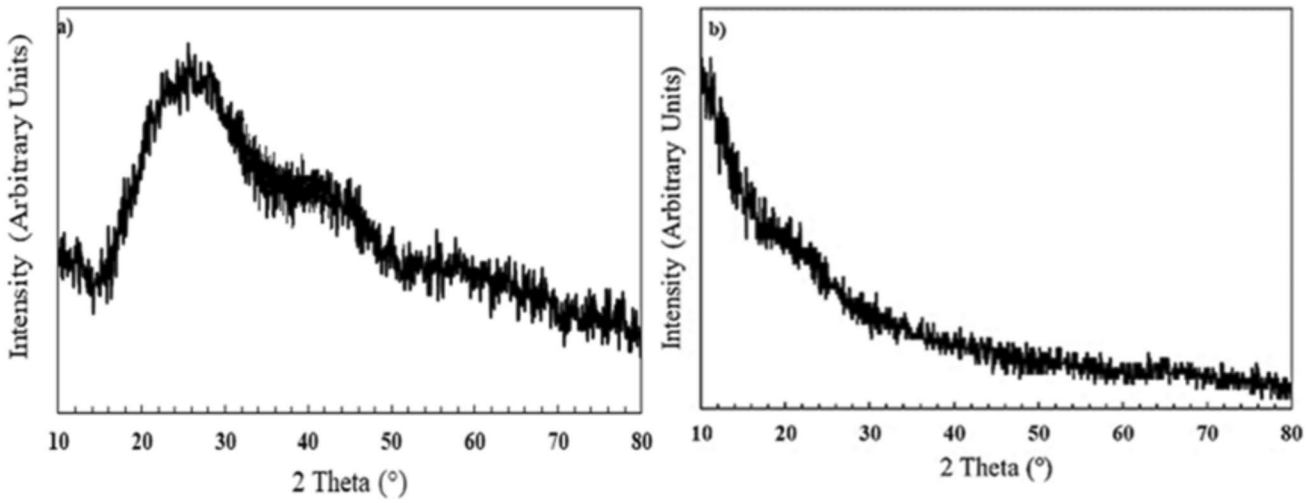

Fig. 1 **a** XRD patterns of the synthesized AlPO4 calcined gel and **b** GI-XRD pattern of aluminum phosphate coated on stainless steel 304 calcined at 500 °C

reference electrode. The working electrode area exposed to the electrolyte was approximately 1 cm^2. Samples were embedded in epoxy resin to expose only the coated surface. These specimens were immersed in each solution for more than 1 h until the open-circuit potential (OCP) was stabilized. Electrochemical impedance spectroscopy (EIS) tests were performed in the frequency range of 100 kHz to 10 mHz with a signal amplitude perturbation of 10 mV at the OCP. The result data was modeled and fitted using ZView software. Potentiodynamic polarization tests were performed from − 250 mV vs. OCP up to the breakdown potential and were terminated at the current density of 10 mA to avoid over-polarization of the reference electrode. To confirm the results, all the electrochemical tests were repeated at least three times.

3 Results and Discussion

3.1 Phase Characterization

According to the XRD patterns shown in Fig. 1a, it can be seen that aluminum phosphate powder has maintained its amorphous structure after heat treatment at 500 °C. In addition, in the GI-XRD pattern of the coating shown in Fig. 1b, no crystalline peaks of $AlPO_4$ or Al_2O_3 can be observed after heat treatment at 500 °C, confirming the XRD results obtained from the calcined powder (Fig. 1a). The stability of the amorphous structure can be related to the excess amount of aluminum as compared to the stoichiometric amount (possibly less than 5%) [19].

3.2 Coating Characterization

The SEM images presented in Fig. 2 show that the amorphous aluminum phosphate coating is uniform and free from cracks and deposits. PVP evaporation in the heat treatment process led to the formation of some porosities on the coating surface. As shown in Fig. 2c, the coating appears as a continuous, crack-free layer between the substrate and the resin. The thickness of the coating, as measured from the image, is approximately 390 nm. The EDS pattern in Fig. 2d shows the presence of aluminum, phosphorus, and oxygen elements on the surface. As shown in Fig. 2d, the coating appears as a continuous, crack-free layer between the substrate and the resin. The thickness of the coating, as measured from the image, is approximately 385 nm.

3.3 Corrosion Resistance in Standard 3.5 wt.% NaCl Solution

3.3.1 Electrochemical Impedance Spectroscopy

Electrochemical tests were conducted to clarify the corrosion resistance of $AlPO_4$ coating and its efficiency in improving the corrosion resistance of AISI 304 stainless steel. The EIS tests were performed in the frequency range of 100 kHz to 10 mHz to evaluate corrosion resistance and the surface quality of the coating.

Figures 3 and 4 show the Nyquist diagrams and the related equivalent circuit used for fitting the results,[2]

[2] All models in this paper are valid for the mentioned frequency range.

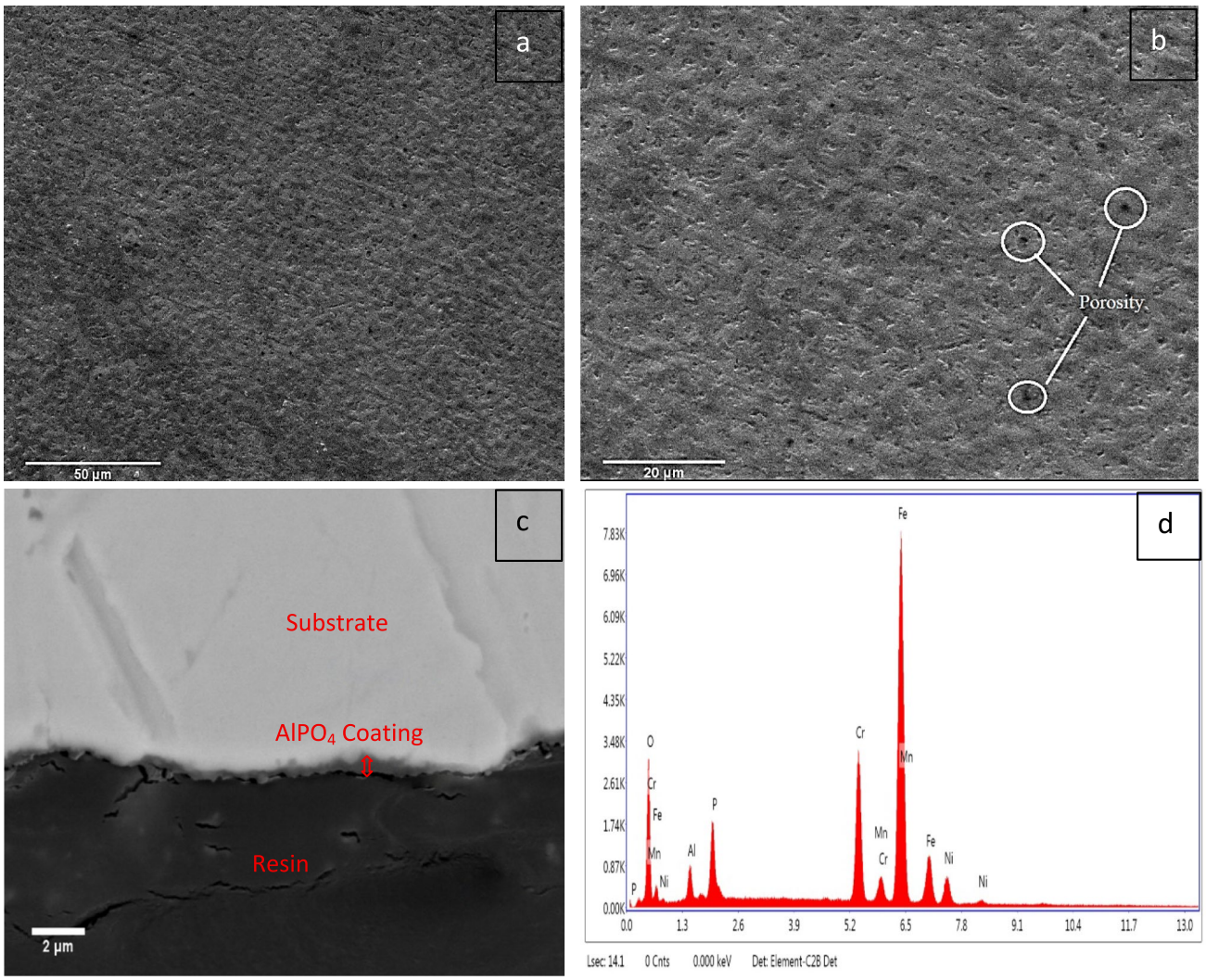

Fig. 2 Scanning electron microscopic images of the coating surface with magnifications, **a** 2000 and **b** 4000 times. **c** Cross-sectional SEM image of the $AlPO_4$ coating on AISI 304 stainless steel. **d** EDS pattern of the coating

respectively. R_s, R_c, R_{ct}, R_{ox}, CPE_c, CPE_{dl}, and CPE_{ox} parameters are related to electrolyte resistance, coating resistance, charge transfer resistance, resistance of oxide layer on the substrate, coating phase constant element capacity, electrical double-layer phase constant element capacity, and oxide layer phase constant element, respectively. The porosity and non-uniformity on the surface result in a local difference between electrochemical activation energy; consequently, the resistance to charge transfer is locally different on the coating surface. For this reason, the capacitive resistance of the coating, and the electric double layer, deviate from the ideal capacitor. Therefore, CPE is used instead of capacitance (C) in the equivalent circuit, and the value of n shows the degree of deviation from the ideal capacitor. The values of parameters obtained from the EIS test are shown in a larger diameter of the semi-circle related to $AlPO_4$ in the Nyquist diagram shown in Fig. 3b, which expresses the impedance value and shows that the resistance of the coating against penetration and impact of the corrosive environment was better than the steel substrate. According to Fig. 3, at high frequencies, the principal mechanism of corrosion resistance is probably related to the diffusion barrier function of the coating against corrosion. Whereas at medium and low frequencies, the electric double layer resists charge transfer [18], which indicates the participation of the coating in corrosion reactions at low frequencies and the filling of porosities with corrosion products.

In the Bode phase diagram shown in Fig. 5a, the presence of a constant phase range indicates the formation of a diffusional impedance due to the formation of a surface layer, indicating non-participation of amorphous aluminum phosphate in corrosion reactions, which, in confirmation of the Nyquist diagram presented in Fig. 3, is the primary corrosion resistance mechanism at high

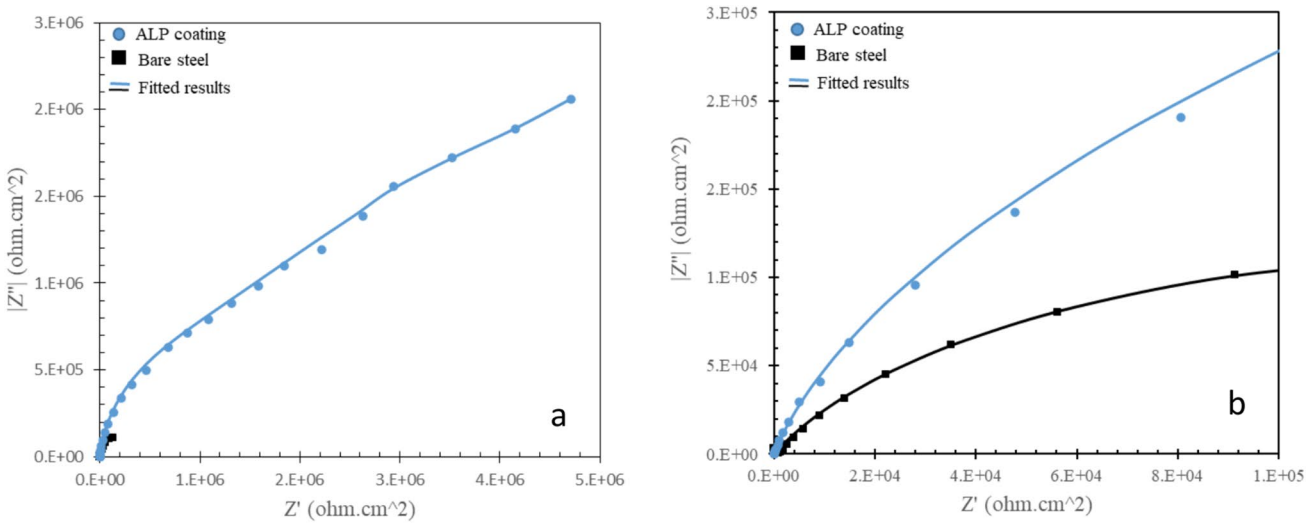

Fig. 3 Nyquist diagram of $AlPO_4$ coating and substrate in 3.5 wt.% NaCl solution **a** real scale and **b** One-tenth scale

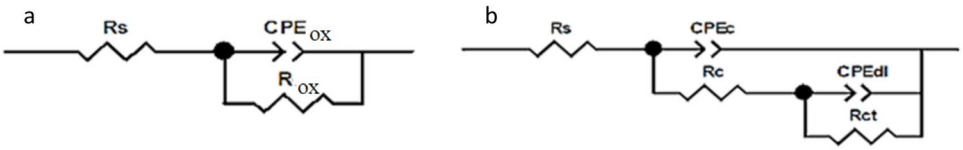

Fig. 4 Equivalent circuit used in modeling. **a** 304 stainless substrates; **b** $AlPO_4$ coating in 3.5 wt.% NaCl solution

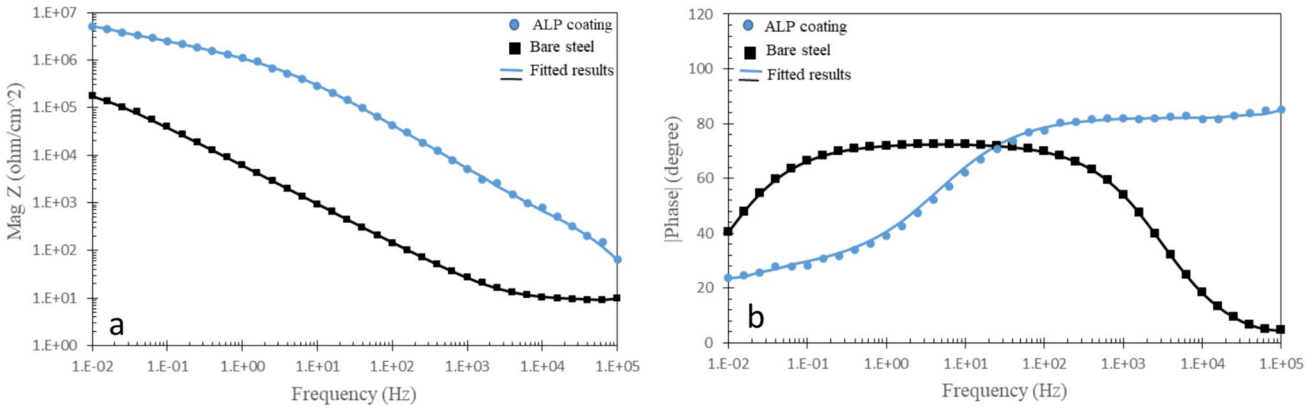

Fig. 5 **a** Bode-Z and **b** Bode-Phase diagrams of $AlPO_4$ coating and 304 stainless steel substrates in 3.5 wt.% NaCl solution

and medium frequencies. As shown in Fig. 5b, the impedance value of the $AlPO_4$ coating, the intersection of the diagram with the vertical axis, is higher than that of the bare substrate. Furthermore, the resistance value at low frequencies for $AlPO_4$ coating is ten times higher than that of the bare substrate, indicating the superiority of the coating against the bare substrate.

3.3.2 Potentiodynamic Polarization

The potentiodynamic polarization test was performed in an aqueous solution of 3.5 wt.% NaCl in the starting potential of − 250 mV versus the OCP of $AlPO_4$ coating and stainless steel substrate. According to the polarization diagram presented in Fig. 6, the corrosion potential (E_{corr}) decreased

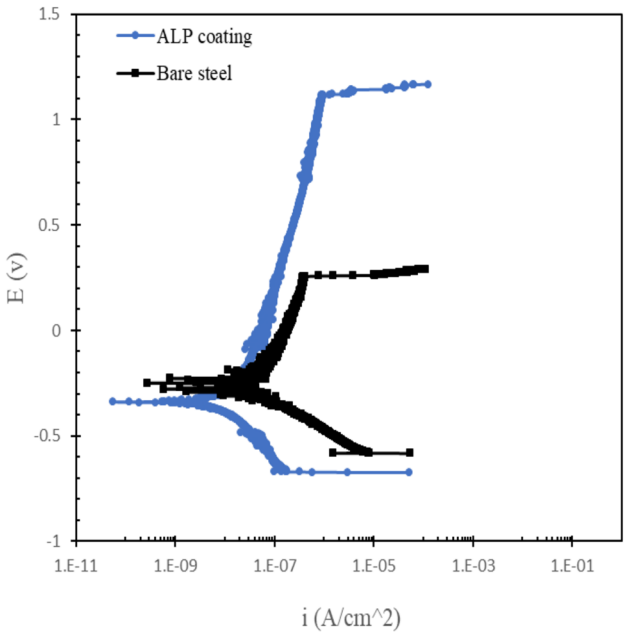

Fig. 6 Potentiodynamic polarization diagram of $AlPO_4$ coating and AISI 304 stainless steel substrate in standard 3.5 wt.% NaCl solution

Table 1 The values of parameters obtained from the EIS test in standard 3.5 wt.% NaCl solution

Sample	Substrate	$AlPO_4$ Coating
R_s (Ohm cm^2)	5.086	5.055
CPE_c (s^n ohm^{-1} cm^{-2})	–	5.96×10^{-8}
n_c	–	0.92
R_c (Ohm.cm^2)	–	4.05×10^{5}
$CPE_{ox/dl}$ (s^n ohm^{-1} cm^{-2})	4.94×10^{-5}	4.59×10^{-7}
$n_{ox/dl}$	0.836	0.38
$R_{ox/ct}$ (Ohm cm^2)	3.25×10^{5}	1.76×10^{7}
Chi-Squared	2.86×10^{-3}	1.75×10^{-3}

from 0.293 $V_{/(Ag/AgCl)}$ corresponding to the substrate to −0.373 $V_{/(Ag/AgCl)}$ for the coating. Corrosion current density (i_{corr}) was also decreased from 5.3×10^{-7} to 9.12×10^{-9} A/cm^2 by $AlPO_4$ coating. With the increase in the potential, the slope of the anodic branch in the diagram of $AlPO_4$ was increased to 0.79, indicating the slow kinetics of $AlPO_4$ corrosion reactions and excellent protective performance. The breakdown potential values (Eb) of the coating and substrate were equal to 1.105 $V_{/(Ag/AgCl)}$ and 0.230 $V_{/(Ag/AgCl)}$, respectively, indicating excellent corrosion resistance even at potentials higher than the breakdown potential of the substrate. According to the anode branch slope of the substrate, which is 0.571 and less than that of the coating, it can be concluded that the coating has much better performance than the protective layer of the substrate and does not participate in corrosion reactions. Table 1 shows the data values extracted from the potentiodynamic polarization test. The polarization resistance was calculated according to the Stern Formula (Eq. 1) [20].

$$\mathrm{Rp} = \frac{\left(\beta_a \times \beta_c\right)}{\left[2.303 \times i_{\mathrm{corr}} \times \left(\beta_a + \beta_c\right)\right]} \tag{1}$$

where Rp represents the polarization resistance, and βa and βc are the slopes of the anodic and cathodic branches, respectively.

The value of this resistance for the $AlPO_4$ coating and the bare substrate was obtained to be 7.4×10^{7} Ω cm^2 and 0.12×10^{6} Ω cm^2, respectively. The difference between the polarization resistance values indicated the excellent performance of the $AlPO_4$ coating in standard 3.5 wt.% NaCl [21]. The protection efficiency coefficient of the coating, which quantitatively shows the effect of coating on the corrosion resistance of the substrate, is calculated by Eq. 2 [5, 22]. Considering that the protection coefficient of $AlPO_4$ coating was equal to 97.4, $AlPO_4$ coating revealed an appropriate protective performance in a wide range of potentials. It shows that it is better than the results obtained from the research of Liu et al. [7], as well as Huang et al. [6].

$$\mathrm{PE}\% = \frac{i^{s}_{\mathrm{corr}} - i^{c}_{\mathrm{corr}}}{i^{s}_{\mathrm{corr}}} \times 100 \tag{2}$$

Since porosity plays a vital role in corrosion resistance, the percentage of coating porosity was calculated by Matthew's formula [20] shown in Eq. 3. In this regard, coatings containing more than 1% porosity do not have sufficient corrosion resistance and quickly corrode and fail [23].

$$P = \frac{{R_{\mathrm{pt}}}/{R_p}^{10^{-|\Delta E_{\mathrm{corr}}|}}}{\beta_a} \times 100 \tag{3}$$

where P is the porosity of the coating, R_{pt} is the polarization resistance of the substrate, R_p is the polarization impedance of the sample to be tested, ΔE_{corr} is the difference in corrosion potential between the substrate and the sample to be tested, and βa is the slope of the anodic polarization curve of the substrate.

From measurements, the value of porosity for coating in standard 3.5 wt.% NaCl solution was obtained to be 0.0096, which is less than the critical value. However, it is possible for the coating to show resistance to even higher potentials as well as lower corrosion current density by reducing the porosity arising from the evaporation of the PVP. As shown in Fig. 7, after the breakdown potential, the coating is severely corroded to the extent that corrosion of

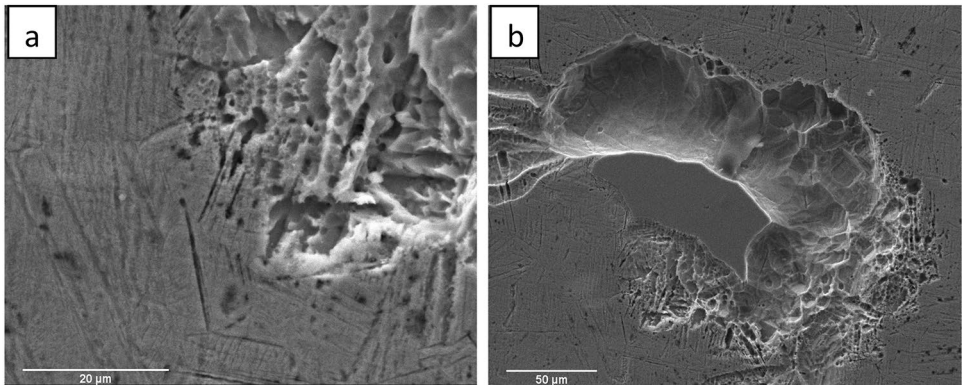

Fig. 7 SEM images of the coating surface after the potentiodynamic polarization test in standard 3.5 wt.% NaCl solution at different magnifications

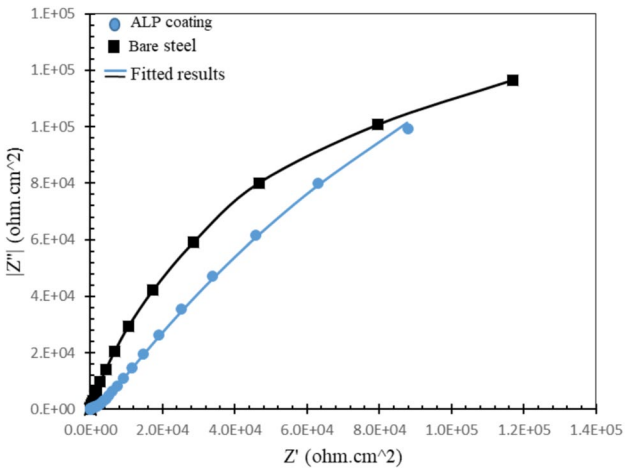

Fig. 8 Nyquist diagram of $AlPO_4$ coating and substrate in industrial H_2SO_4 solution

the substrate can also be seen in some areas (Fig. 7a). In addition, small cracks and relatively deep pits can also be seen in Fig. 7b.

3.4 Corrosion Resistance in Industrial Sulfuric Acid Solution

3.4.1 Electrochemical Impedance Spectroscopy

According to the small ring that can be seen at the beginning of the Nyquist diagram in Fig. 8, it can be concluded that the mechanism of corrosion resistance and electrolyte penetration in an acidic environment is very different from a saline environment. An increase in the number of concavities and convexities in the bode-phase diagram in Fig. 9a compared to standard 3.5 wt.% NaCl solution indicates a difference in the corrosion mechanism. The equivalent circuit that was considered for modeling the EIS results includes two series loops related to the copper film and the coating and one parallel loop related to the electrochemical double layer [24]. The equivalent circuit is shown in Fig. 10, and the parameters R_s, R_C, R_f, R_{ct}, R_{ox}, CPE_f, CPE_c, $CPE_{ox,}$ and CPE_{dl} are respectively related to electrolyte resistance, coating resistance, resistance of oxide layer on the substrate, film resistance (possibly a Cu film on the coating), charge transfer resistance, the phase constant element of the coating acting as a diffusion barrier, the phase constant element

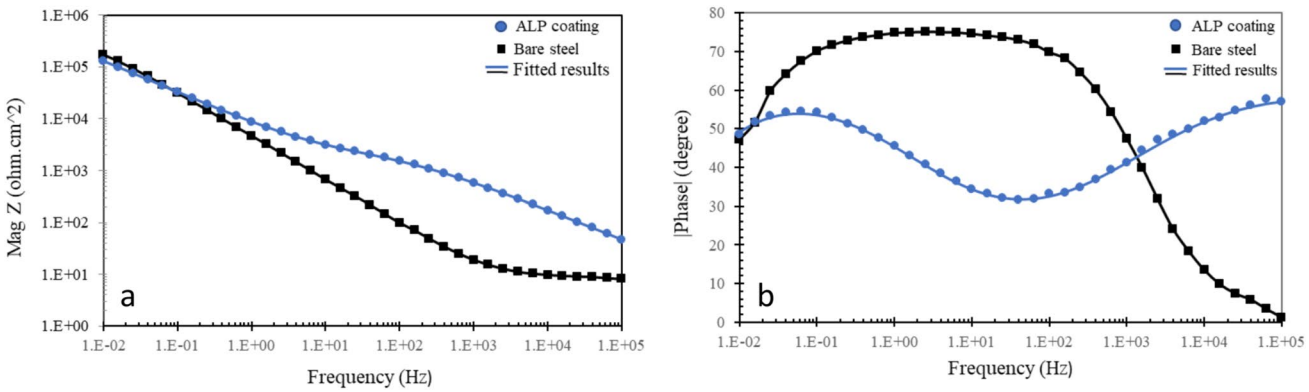

Fig. 9 **a** Bode-Z and **b** Bode-phase diagrams of $AlPO_4$ coating and AISI 304 stainless steel substrate in industrial H_2SO_4 solution

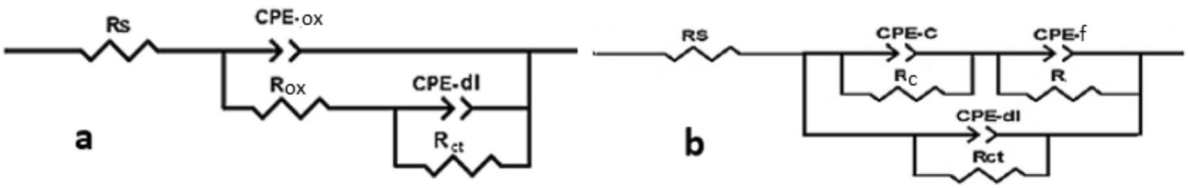

Fig. 10 The equivalent circuit used in modeling **a** 304 stainless substrates; **b** $AlPO_4$ coating in industrial H_2SO_4 solution

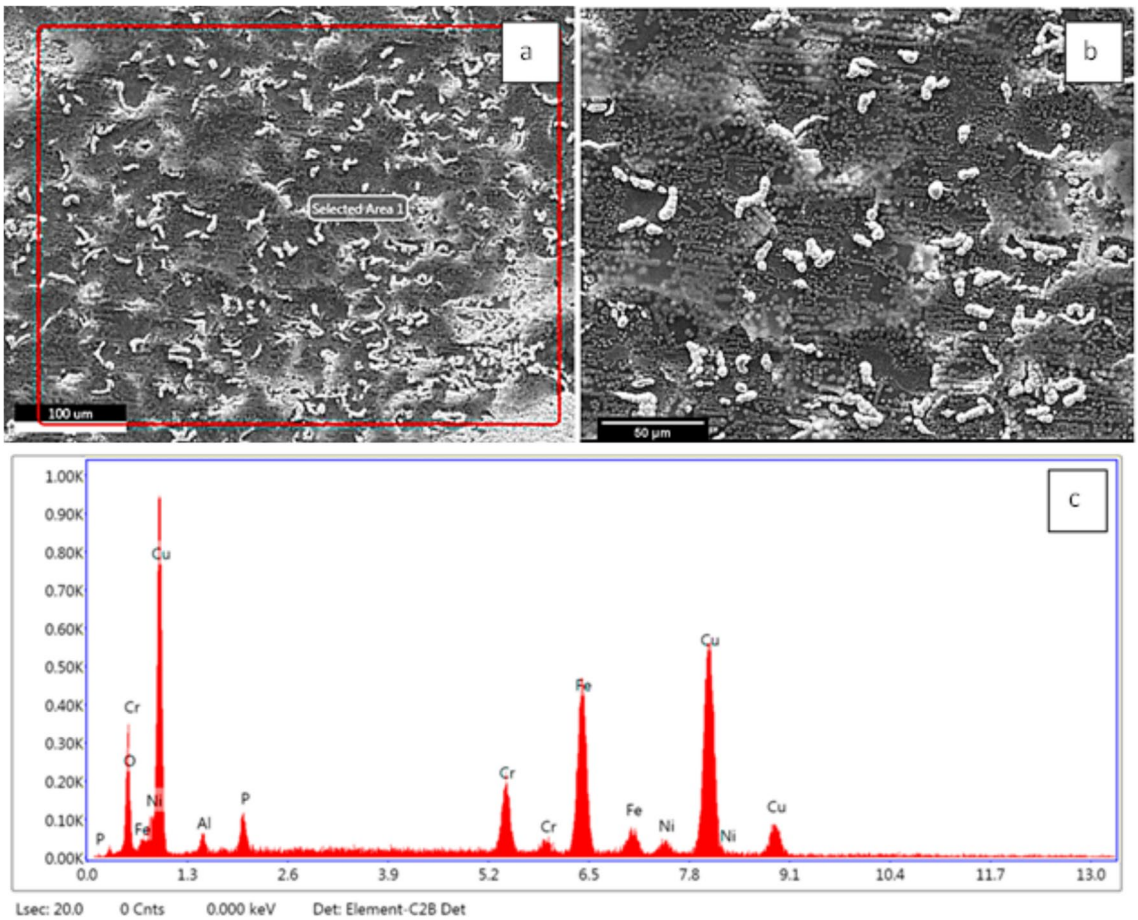

Fig. 11 **a** SEM images of the coating surface after the potentiodynamic polarization test in industrial H_2SO_4 solution, **b** selected for the EDS test, and **c** EDS test results

of the oxide layer, the phase constant element of the film, and the phase constant element of the electric double layer [25]. According to the SEM image and the EDS pattern of the coating presented in Fig. 11, a copper film has been deposited on the surface after the electrochemical corrosion test. The source of Cu is probably due to the contaminated industrial acidic solution obtained from the copper refinery. Considering the galvanic series, copper deposition on steel is a spontaneous reaction. In this reaction, copper tends to

Table 2 The values of the parameters obtained from the potentiodynamic polarization test in standard 3.5 wt.% NaCl solution

Sample	Substrate	$AlPO_4$ coating
E_{corr} ($V_{/(Ag/AgCl)}$)	−0.293	−0.373
i_{corr} (A/cm^2)	3.5×10^{-7}	9.12×10^{-9}
R_P (Ωcm^2)	1.2×10^{5}	4.7×10^{7}
PE%	–	97.4
P	–	9.6×10^{-3}

be reduced and deposited in the bare steel, areas in which coating has been lost due to defects or corrosion reactions. According to the Nyquist diagram and EIS parameter values presented in Table 2, the coating loses its barrier properties at lower frequencies, and the charge transfer mechanism comes into play. In the substrate, the corrosion mechanism includes the protective film formed during corrosion reactions and charge transfer resistance from the electrical double layer. The bode-Z diagram (Fig. 9b) shows that the coating impedance is higher than that of the bare substrate.

Due to the lack of research on the corrosion behavior of this coating in an acidic environment, to validate the considered model, the effective capacitance was estimated through the following equation [25, 26].

$$C_{\text{eff}} = C^{\frac{1}{n}} \left(\frac{1}{R_c} \right)^{\frac{n-1}{n}} \tag{4}$$

where C and n are the CPE elements related to the coating and Rc is the coating resistance. Using the values in Table 3, the effective capacitance value was calculated as 2.16×10^{-7}. In addition, using the value of effective capacity, the coating thickness was calculated from the following equation:

$$I_C = \frac{\varepsilon \varepsilon_0 A}{C_{\text{eff}}} \tag{5}$$

where ε_0 is the permittivity of the vacuum, with the value of 8.85×10^{-14} F cm^{-1}, ε is the relative permittivity and it was set to 2.3 [13, 26], A is the effective surface of the sample (cm^2) and C is the simulated effective capacitance of the coating. The theoretical thickness of the coating, estimated from the dielectric model (Eqs. 4 and 5), was approximately 384 nm. This value is in good agreement with the actual thickness measured in the cross-sectional SEM image (Fig. 2c), further validating the accuracy of the electrochemical model used [12].

Table 3 The values of parameters obtained from the EIS test in industrial H_2SO_4 solution

Sample	Substrate	$AlPO_4$ coating
R_s (Ohm cm^2)	5.09	4.062
$CPE_{ox/c}$ (s^n ohm^{-1} cm^{-2})	4.5×10^{-5}	3.91×10^{-7}
$n_{ox/c}$	0.83	0.92
$R_{ox/c}$ (Ohm cm^2)	47,734	2728
CPE_f (s^n ohm^{-1} cm^{-2})	–	3.14×10^{-5}
N_f	–	0.62
R_f (Ohm cm^2)	–	5.86×10^5
CPE_{dl} (s^n ohm^{-1} cm^{-2})	4.9×10^{-7}	9.86×10^{-6}
n_{dl}	0.43	0.56
R_{ct} (Ohm.cm^2)	4.01×10^5	6.97×10^6
Chi-Squared	1.47×10^{-3}	1.05×10^{-3}

3.4.2 Potentiodynamic Polarization Curves

The polarization curve for aluminum phosphate-coated AISI 304 stainless steel, as well as the bare AISI 304 stainless steel was plotted and analyzed using the electrochemical polarization test results. According to the polarization diagram presented in Fig. 12, in an acidic solution, the corrosion potential is positive both in the substrate and in the $AlPO_4$ coating. It is worth noting that, the OCP of the $AlPO_4$-coated sample shifted negatively in the NaCl environment, while it moved toward more positive values in the acidic medium. This contrast can be attributed to the nature of corrosion reactions in each environment. In NaCl, the coating primarily acts as a passive diffusion barrier, suppressing anodic activity and shifting the OCP in the cathodic direction. In contrast, in the industrial H_2SO_4 solution, spontaneous deposition of a copper-rich layer on exposed areas creates a galvanic shift toward anodic potentials. Similar trends were reported in literature investigating coating-electrolyte interactions in aggressive media [27–29]

Corrosion potential values for the aluminum phosphate coating and AISI 304 steel substrate are 0.308 $V_{/(Ag/AgCl)}$ and 0.113 $V_{/(Ag/AgCl)}$, respectively, and corrosion current density values are 1.58×10^{-7} A/cm^2 and 1.67×10^{-6} A/cm^2, respectively. The lower corrosion current density value in the industrial sulfuric acid solution for the coated steel as

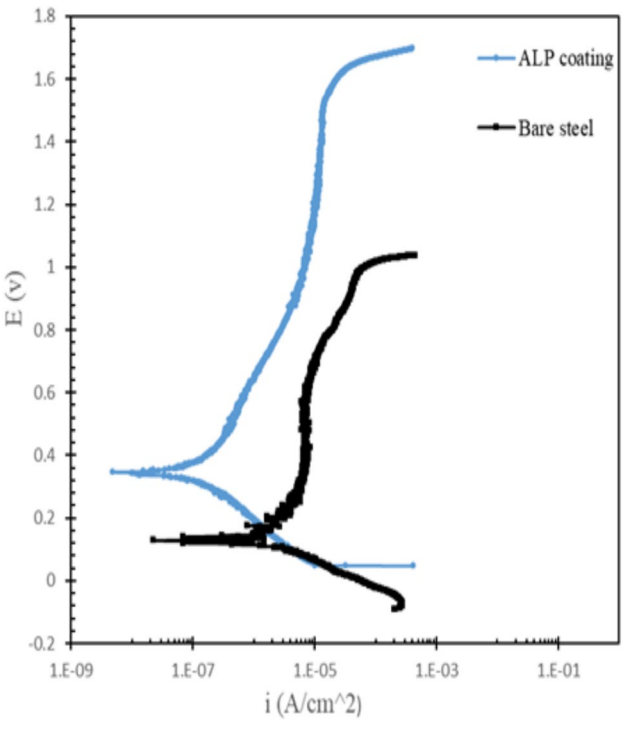

Fig. 12 Potentiodynamic polarization diagram of $AlPO_4$ coating and AISI 304 stainless steel substrate in industrial H_2SO_4

Table 4 The values of the parameters obtained from the potentiodynamic polarization test in industrial H_2SO_4 solution

Sample	Substrate	$AlPO_4$ coating
E_{corr} ($V_{/(Ag/AgCl)}$)	0.113	0.308
i_{corr} (A/cm^2)	1.67×10^{-6}	1.58×10^{-7}
R_P (Ωcm^2)	1.8×10^{4}	2.9×10^{5}
P	–	0.089
PE%	–	90.5

compared to bare steel, indicates the slower corrosion reactions' kinetics.

The value of breakdown potential for the aluminum phosphate-coated steel and substrate was 1.538 $V_{/(Ag/AgCl)}$ and 0.967 $V_{/(Ag/AgCl)}$, respectively, indicating higher stability of the protective layer formed at higher potentials. The values of the coating and substrate's polarization resistance and the coefficient of protective effect in an acidic environment are equal to 9.2×10^5 Ω cm^2, 2 1.8×10^5 Ω cm^2, and 90%, respectively. The coating porosity percentage was calculated and the value of the parameter, which is 0.089, indicates that porosities are more active in the acidic environment, but do not fail the coating. The data extracted from the potentiodynamic polarization test in the acidic environment are summarized in Table 4, which in general, shows that the $AlPO_4$ coating has acceptable corrosion performance in the industrial sulfuric acid solution as compared to bare metal, and could be used to protect the AISI 304 substrate against corrosion in the mentioned environment, and a wide range of potentials.

4 Conclusions

- A uniform amorphous crack-free aluminum phosphate coating was applied on AISI 304 steel substrate through a sol–gel process following heat treatment at 500 °C. Although the coating was uniform and crack-free, it contained some porosities due to the evaporation of PVP during the heat treatment.
- The corrosion resistance of the amorphous aluminum coating was superior in both the standard 3.5% NaCl solution as well as the industrial sulfuric acid solution, as compared to AISI 304 stainless steel base material. This was mainly due to the ceramic base nature, as well as the amorphous nature of the coating.
- The mechanism of corrosion resistance for the amorphous aluminum phosphate coating was different depending on the environment. In fact for the standard 3.5% NaCl solution, the coating acted as a diffusion barrier, but in the industrial H_2SO_4 solution, the corrosion resistance mechanism included a combination of the diffusion barrier mechanism of the coating and the formation of a Cu film due to the spontaneous reaction of Cu reduction on steel, at the same time.

Acknowledgements The authors would like to acknowledge the support provided by the Isfahan University of Technology and the Department of Materials Engineering.

Author Contributions All authors contributed to the study's conception and design. Material preparation, data collection, and analysis were performed by [Tara Bazdar]. The first draft of the manuscript was written by [Tara Bazdar] and all authors commented on previous versions of the manuscript. All authors read and approved the final manuscript.

Funding The authors declare that no funds, grants, or other support were received during the preparation of this manuscript.

Data Availability No datasets were generated or analysed during the current study.

Declarations

Conflict of Interests The authors declare no conflict of interests.

References

1. He Y (2020) Wireless corrosion monitoring sensors based on electromagnetic interference shielding of RFID transponders. Corrosion 76:411–423
2. Hawthorne HM, Neville A, Troczynski T et al (2004) Characterization of chemically bonded composite sol–gel based alumina coatings on steel substrates. Surf Coat Technol 176:243–252. https://doi.org/10.1016/S0257-8972(03)00663-7
3. Lin YJ, Tu SH (2009) Joining of mullite ceramics with yttrium aluminosilicate glass interlayers. Ceram Int 35:1311–1315. https://doi.org/10.1016/J.CERAMINT.2008.06.006
4. Ye K, Li Z (2020) Toward ceramic anticorrosion coatings: a review. Corrosion 76:895–917. https://doi.org/10.5006/3560
5. Bian D, Zhao Y (2016) Preparation and corrosion mechanism of graphene-reinforced chemically bonded phosphate ceramics. J Solgel Sci Technol 80:30–37
6. Huang X, Wang D, Dong Y (2020) Corrosion resistance phosphate coating formed by steam assisted curing on cast AlSi alloy. Surf Coat Technol 382:125242
7. Liu Y, Bian D, Zhao Y (2019) The influence of curing agents on thermal property and corrosion resistance of chemically bonded phosphate ceramic coatings. J Solgel Sci Technol 89:403–415. https://doi.org/10.1007/s10971-018-4907-4
8. Ding Z, Li Y-Y, Xu M-R et al (2020) Electrochemical properties of aluminum tripolyphosphate modified chemically bonded phosphate ceramic anticorrosion coating. Constr Build Mater 251:118874
9. Wagh AS, Jeong SY (2003) Chemically bonded phosphate ceramics: I, a dissolution model of formation. J Am Ceram Soc 86:1838–1844
10. Wagh AS (2013) Recent progress in chemically bonded phosphate ceramics. Int Sch Res Notices. https://doi.org/10.1155/2013/983731
11. Kingery WD (1950) Fundamental study of phosphate bonding in refractories: I, literature review. J Am Ceram Soc 33:239–241. https://doi.org/10.1111/j.1151-2916.1950.tb14171.x

12. Sayyedan FS, Enayati MH (2018) Evaluating oxidation behavior of amorphous aluminum phosphate coating. Appl Surf Sci 455:821–830. https://doi.org/10.1016/j.apsusc.2018.06.087
13. Sambasivan S, Steiner KA, Rangan KK (2010) Aluminum phosphate coatings
14. Muraoka Y, Kihara K (1997) The temperature dependence of the crystal structure of berlinite, a quartz-type form of AlPO4. Phys Chem Miner 24:243–253
15. Lang R, Calvo C, Datars WR (1977) Phase transformation in AlPO4 and quartz studied by electron paramagnetic resonance of Fe3+. Can J Phys 55:1613–1620
16. Maharana R, Raja MM, Prasad VVB et al (2014) Synthesis and study of magnetic properties of high temperature stable Ni nanoparticles in a nearly amorphous $AlPO_4$ matrix in an oxidative atmosphere. J Mater Chem C 2:5142–5148. https://doi.org/10.1039/C4TC00604F
17. Li N, Zhong M, Xu Z, Zhang Z (2018) Polyesterification synthesis of amorphous aluminum phosphate thermal radiation material with high infrared emissivity. Mater Lett 213:335–337. https://doi.org/10.1016/j.matlet.2017.11.048
18. Sayyedan F, Enayati M, Taghipour M, Ghasemizadeh P (2023) Corrosion resistance of amorphous $AlPO_4$ coating in salty atmospheres. J Chin Chem Soc. https://doi.org/10.1002/jccs.202300039
19. Sayyedan FS, Enayati MH (2019) On structure and oxidation behaviour of non-stoichiometric amorphous aluminium phosphate coating. Surf Eng 35:670–676. https://doi.org/10.1080/02670844.2018.1560912
20. Mansfeld F (1976) The polarization resistance technique for measuring corrosion currents. Adv Corros Sci Technol 6:163–262
21. Liu X, Xiong J, Lv Y, Zuo Y (2009) Study on corrosion electrochemical behavior of several different coating systems by EIS. Prog Org Coat 64:497–503
22. Shao F, Yang K, Zhao H et al (2015) Effects of inorganic sealant and brief heat treatments on corrosion behavior of plasma sprayed Cr2O3–Al2O3 composite ceramic coatings. Surf Coat Technol 276:8–15
23. Jiejing C, Hong JU, Can SUN et al (2017) Application of electrochemical testing technology for corrosion under-deposits. J Chin Soc Corros Protect 37:207–215
24. Mopon ML, Garcia JS, Manguerra DM, Narisma CJC (2021) Corrosion behavior of aa 1100 anodized in gallic-sulfuric acid solution. Coatings. https://doi.org/10.3390/coatings11040405
25. Hirschorn B, Orazem ME, Tribollet B et al (2010) Constant-phase-element behavior caused by resistivity distributions in films. J Electrochem Soc 157:C452. https://doi.org/10.1149/1.3499564
26. Yuan X, Yue ZF, Chen X et al (2015) EIS study of effective capacitance and water uptake behaviors of silicone-epoxy hybrid coatings on mild steel. Prog Org Coat 86:41–48. https://doi.org/10.1016/j.porgcoat.2015.04.004
27. Grzesik Z, Mrowec S (2008) On the sulphidation mechanism of niobium and some of Nb-alloys at high temperatures. Corros Sci 50:605–613. https://doi.org/10.1016/j.corsci.2007.09.007
28. Choi Y-S, Kim J-G (2009) Determination of cathodic protection potential criteria for thermally insulated pipeline in synthetic groundwater. Corrosion 65:88–95. https://doi.org/10.5006/1.3319123
29. Tsou H-K, Hsieh P-Y, Chung C-J et al (2009) Low-temperature deposition of anatase TiO2 on medical grade polyetheretherketone to assist osseous integration. Surf Coat Technol 204:1121–1125. https://doi.org/10.1016/j.surfcoat.2009.06.018